Intangible Hydrodynamic Cloaks for Convective Flows

Bin Wang,[1,2,*] Tien-Mo Shih,[3] Liujun Xu,[1] Gaole Dai,[4] and Jiping Huang[1,†]

[1] *Department of Physics, State Key Laboratory of Surface Physics, and Key Laboratory of Micro and Nano Photonic Structures (MOE), Fudan University, Shanghai 200438, China*

[2] *School of Mechanical and Power Engineering, East China University of Science and Technology, Shanghai 200237, China*

[3] *Department of Mechanical Engineering, University of California, Berkeley, CA 94720, USA*

[4] *School of Sciences, Nantong University, Nantong 226019, China*

(Received 12 December 2019; revised 5 February 2021; accepted 10 February 2021; published 4 March 2021)

Although studies of hydrodynamic cloaking have attracted considerable attention, most pioneering studies have so far focused on creeping flows, in which nonlinear convective terms are neglected and cloaks are fabricated with inhomogeneous or anisotropic metamaterials. Here we discover that intangible uniform-viscosity hydrodynamic cloaks, which are capable of hiding obstacles immersed in narrow-gap Navier-Stokes flows with non-negligible convection, can be possibly designed. Via the convection-diffusion-balance method and the realizable thermally controlled tactic, the diffusion effect exerted by the obstacle surface can be balanced by the convection counterpart exerted by the manipulation of temperature-dependent viscosity inside the intangible cloak. This analysis has been validated by finite-element computational simulations that tackle cloaked-cylinder flows for Reynolds numbers in the laminar regime. The proposed study may lay the foundation for attempts to further explore hydrodynamic cloaks and possibly other metamaterial-related devices.

DOI: 10.1103/PhysRevApplied.15.034014

I. INTRODUCTION

Objects moving in viscous fluids will inevitably interfere with flow fields, rendering the manipulation of attenuating interferences challenging. With inspiring developments of extensive metamaterials, substantial interests arose in fabricating cloaking devices to hide objects that were immersed in external physical fields, such as light [1–4], electromagnetism [5–9], acoustics [7,10,11], dc electrics [12], solid mechanics [13,14], conductive heat transfer [15–18], liquid waves [19–21], and quantum-mechanical matter waves [22,23], among others. Urzhumov *et al.* [24] began to pay attention to porous-media hydrodynamic cloaks, which were first designed on the basis of coordinate transformations of Darcy's pressure equation and the Brinkman-Stokes equation for creeping flows. Hereafter, numerous investigators [25–29] devoted their efforts on hydrodynamic metamaterials in porous media.

Recently, Park *et al.* [30] proposed a hydrodynamic metamaterial cloak by utilizing the transformation theory for Stokes flows in the non-porous-media hydrodynamic space, creating a concept that treated the viscosity as a tensor. However, these hydrodynamic metamaterials were designed by microstructures with inhomogeneous and anisotropic properties, leading to somewhat sophisticated fabrications of these metamaterials. Furthermore, a metamaterial-free hydrodynamic cloak was designed by Tay *et al.* [31], who optimized the height of the cylinder shell to cloak objects. Also notably, because nonlinear convective terms are omitted [30,31], these creeping flows are governed by Stokes equations.

Facing these challenges mentioned above, we manage to investigate intangible uniform-viscosity hydrodynamic cloaks by using the convection-diffusion-balance method and by varying the dynamic viscosity of the fluid, enabling us to manipulate viscous non-negligible-convection Navier-Stokes flows around obstacles. To validate the cloaking analysis, we conduct computational simulations by using the commercial package COMSOL.

II. PHYSICAL MODELS AND ANALYTICAL RESULTS

Consider a horizontally situated cylindrical obstacle [Figs. 1(a) and 1(b)] with radius R_1 impermeable to the fluid (regime III). It is surrounded by a concentric cloak shell (regime II) of exterior radius R_2, steadily immersed in a freestream (regime I), with an incoming velocity v_{in}

*bwang@ecust.edu.cn
†jphuang@fudan.edu.cn

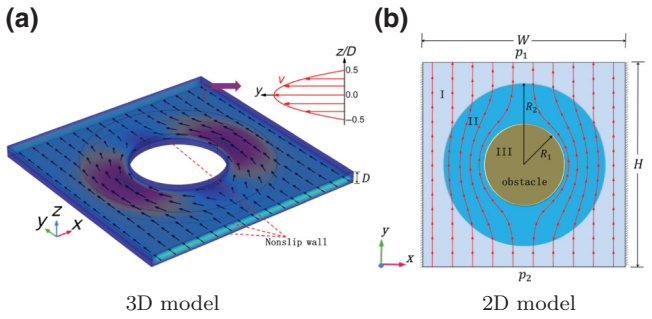

FIG. 1. Schematic models of a hydrodynamic cloaks. Geometry with height (H) × width (W) × depth (D) = 1 cm × 1 cm × 50 μm, $R_1 = 2$ mm, and $R_2 = 4$ mm. The radius of the obstacle and the outside radius of the cloak are R_1 and R_2, respectively. Water with the dynamic viscosity $\mu = 1$ mPa s and the density $\rho = 997.1$ kg/m^3 at room temperature are chosen as the working fluid. (a) Three-dimensional (3D) model with parabolic velocity profiles on the y-z plane. (b) Two-dimensional (2D) model.

in the y direction predetermined by a pressure gradient of $\triangle p$ ($p_2 > p_1$). Nonslip boundary conditions are applied to surfaces of all solid walls in the domain within $x = \pm 0.5W$, $z = \pm 0.5D$, and $r = R_1$. If the cloaking process is accomplished, the fluid will move as if no obstacle exists.

The continuity equation and Navier-Stokes equations for incompressible flows at steady state without the influence of body forces can be written as

$$\nabla \cdot \mathbf{u} = 0, \tag{1}$$

$$\rho \mathbf{u} \cdot \nabla \mathbf{u} + \nabla p = \nabla \cdot (\mu \nabla \mathbf{u}), \tag{2}$$

where ρ, μ, $\mathbf{u}$, and p denote density, dynamic viscosity, velocity vector, and pressure, respectively.

According to derivations in Appendix A (Part 1), under irrotational-flow idealization, Eqs. (1) and (2) can be transformed into Laplace equations as

$$\nabla \cdot \nabla \varphi = 0, \tag{3}$$

$$\nabla \cdot \left(\mu^{-1} \nabla Q\right) = 0, \tag{4}$$

where φ satisfies $\nabla \varphi = \mathbf{u}$, known as the velocity potential, and $Q = \frac{1}{2}\rho|\mathbf{u}|^2 + p$. Here the term $\frac{1}{2}\rho|\mathbf{u}|^2$ in $Q = \frac{1}{2}\rho|\mathbf{u}|^2 + p$ originates from the nonlinear convective term $\mathbf{u} \cdot \nabla \mathbf{u}$ and bears the unit of mechanical energy density (J/m^3). Equations (3) and (4) contain two field variables, φ and Q, instead of four primitive counterparts contained in Eqs. (1) and (2), namely $\mathbf{u}$ (three directions in x, y, z) and p, facilitating the analysis and the computation. Furthermore, Eqs. (3) and (4) can be unified into

$$\nabla \cdot (\xi \nabla \Theta) = 0, \tag{5}$$

where $\xi = \left(1, \mu^{-1}\right)$ and $\Theta = (\varphi, Q)$.

Herein, since Eq. (5) bears the Laplace-equation form, an analytical solution can be obtained by using separation of variables [8,32–35].

In the proposed study, as long as the globally effective dynamic viscosity of both the obstacle and the cloak equals that for the freestream (μ_{I}), the purpose of the cloaking has been attained. This treatment takes advantage of the concept, in which the diffusion effect exerted by the obstacle surface can be balanced by the convection effect exerted within the cloak. Hence, it is tentatively named the "convection-diffusion-balance method".

Treating the viscosity at the solid obstacle surface as $\mu_{\mathrm{III}} = \infty$, we can obtain the uniform dynamic viscosity of the cloak as

$$\mu_{\mathrm{II}} = \frac{R_2^2 - R_1^2}{R_2^2 + R_1^2}\mu_{\mathrm{I}} \qquad R_1 < r \leq R_2, \tag{6}$$

where μ_{I} denotes the dynamic viscosity of the freestream. The derivation of Eq. (6) is shown in Part 2 of Appendix A. From Eq. (6), we can observe that μ_{II} can be purely determined in terms of values of R_1, R_2, and μ_{I}, but not in terms of spatial coordinates.

III. NUMERICAL SIMULATIONS

According to Refs. [36,37], a viscous flow in a narrow gap between two parallel plates in z direction ($D \ll H$ and W) behaves similarly as an inviscid fluid does in the x-y plane. Therefore, vorticities produced by the nonslip condition in the x-y plane exist only inside the boundary layer and will not diffuse into the flow from all obstacle walls on the $z = 0$ plane in a certain range of Reynolds numbers [Fig. 7(a)]. Additionally, since nonslip conditions are prescribed on $z = \pm 0.5D$ planes, the flow exhibits parabolic-flow characteristics in y-z planes [inset of Fig. 1(a)]. For $z \neq 0$ planes, although vorticities do not equal zero at the entire plane, these parabolic velocities are mirror symmetrical with respect to the $z = 0$ plane. Subsequently, vorticities on, for example, the $z = 0.2D$ plane (or $0.4D$ plane) and those on $z = -0.2D$ plane (or the $-0.4D$ plane) bear the same values but different signs [Figs. 7(b) and 7(c)], and thus will balance each other. Therefore, these flows can be treated as nearly globally irrotational ones (i.e., viscous potential flows), and applications of our cloak can be considered valid.

Based on Eqs. (1) and (2) and Eq. (6), computational simulations are conducted to validate our analysis for the fabrication of hydrodynamic cloaks using COMSOL Multiphysics, a commercial finite-element package.

At first we consider flows with a small Re, $\mathrm{Re} = \rho v_{\mathrm{in}} D/\mu = 1.03$ (Fig. 2). For the obstacle-absent case, streamlines and isobars of the velocity field intersect orthogonally, and the velocity field behaves almost as uniformly as the quasi-inviscid flow does because of $D \ll H$

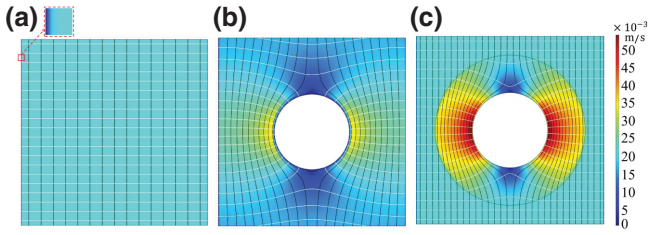

FIG. 2. Velocity distributions superimposed with streamlines (black color) and isobars (white color) on the $z = 0$ plane at Re = 1.03. (a) Obstacle absent, (b) obstacle existent, (c) cloaking.

and W. It should be noted that, realistically, boundary layers do exist near vertical walls on both sides, and that the flow remains viscous [inset of Fig. 2(a)].

For the obstacle-existent case, the solid obstacle can be equivalently treated as an effective infinitely-viscous fluid that retards flows, leading to the phenomenon in which streamlines and isobars are conspicuously distorted [Fig. 2(b)].

To cancel these effects of obstruction, we bring the proposed hydrodynamic cloak to cover the bare obstacle. Because of $\mu_{\mathrm{II}} < \mu_{\mathrm{I}}$ according to Eq. (6), the boundary-layer flow, which would have existed in the presence of the obstacle, has now diminished. Under these circumstances, the cloak does function to artificially enhance the convection that surrounds the obstacle [Fig. 2(c)]. In this sense, the cloak is capable of behaving as if the overall viscosity around it takes the value of the freestream viscosity. In other words, streamlines and isobars outside the cloak shown in Fig. 2(a) and those in Fig. 2(c) equal each other. On the $z \neq 0$ plane, distributions of streamlines and isobars resemble those on the $z = 0$ plane except for magnitudes [shown in Figs. 5(d)–5(f) for different Re's].

As Re increases, the effect of nonlinear convective term $\rho\mathbf{u} \cdot \nabla\mathbf{u}$ in the equation gradually emerges. To investigate this effect on the cloaking, we need only to examine the orthogonality between streamlines and isobars outside the cloak because these two families of lines for the obstacle-absent case at different Re's look similar to one another.

Next, velocity distributions superimposed with streamlines (black lines) and isobars (white lines) at various laminar Re's are presented in Figs. 3(a)–3(d). The orthogonality between straight streamlines and isobars can be observed outside the cloak at higher Re's.

To further quantitatively check the validity of cloaking schemes, we compare y-component velocity at three points (v_a, v_b, v_c) near the cloak surface with the inlet velocity (v_{in}) in Fig. 4. As Re increases, values of v_a, v_b, and v_c continue to equal that of v_{in}. It is worthwhile to note that, at higher Re's, e.g., $25 \leq \mathrm{Re} \leq 43$, v_a and v_b basically coincide with v_{in}, whereas v_c slightly deviates from v_{in} within the error tolerance. To clearly understand mechanisms of these deviations, we first show pressure distributions on the cylinder surface [Figs. 8(a) and 8(b)]. For $1 < \mathrm{Re} \leq 43$, as Re increases, the effect of the nonlinear convective term $\rho\mathbf{u} \cdot \nabla\mathbf{u}$ (which constitutes two parts $\frac{1}{2}\rho\nabla|\mathbf{u}|^2$ and $\rho\mathbf{u} \times \nabla \times \mathbf{u}$) gradually emerges and pressure distributions on the cylinder surface gradually become asymmetric. However, the symmetry of the velocity field [Fig. 8(c)] nearly remains, and the vorticity on the $z = 0$ plane continues to be primarily bounded in the cylindrical boundary layer [Fig. 8(d)]. These phenomena suggest that the effect of the kinetic term ($\frac{1}{2}\rho\nabla|\mathbf{u}|^2$) starts emerging but the effect of the rotational term ($\rho\mathbf{u} \times \nabla \times \mathbf{u}$) can be omitted outside the boundary layer. Therefore, within the error tolerance, the flow irrotationality can continue to be acknowledged. Consequently, our cloak can be considered valid under $\mathrm{Re} \leq 43$. As Re continues to increase, the fore-aft symmetry of the pressure [Fig. 8(b)] and that of the velocity [Fig. 8(e)] gradually breaks down. (We choose a relatively large Re = 159.38 as a stark comparison.) Under this circumstance, the vorticity escapes from the constraint of the boundary layer [Fig. 8(f)]. Hence, our cloak gradually becomes invalid.

Characteristics exhibited in both Figs. 2–4 imply that the cloaked obstacle has hardly distorted the velocity field or reduced the magnitude of the velocity outside the cloak, thereby indicating that the hydrodynamic cloak is valid in a certain range of Re's.

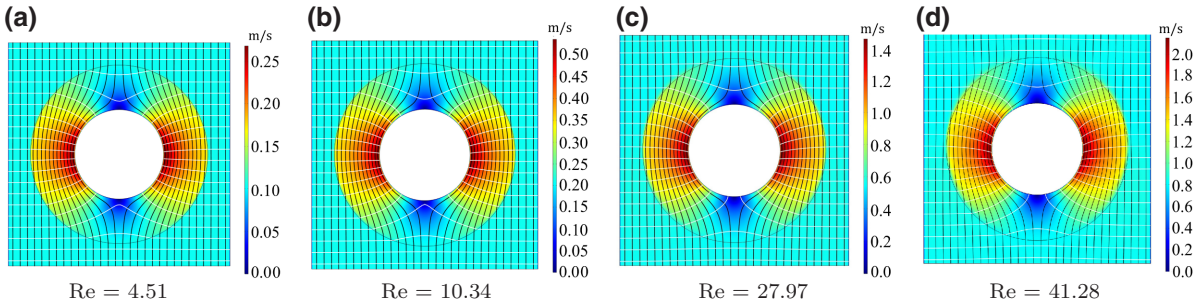

FIG. 3. Velocity distributions superimposed with streamlines (black lines) and isobars (white lines) of the hydrodynamic cloak on the $z = 0$ plane at various laminar large Re's.

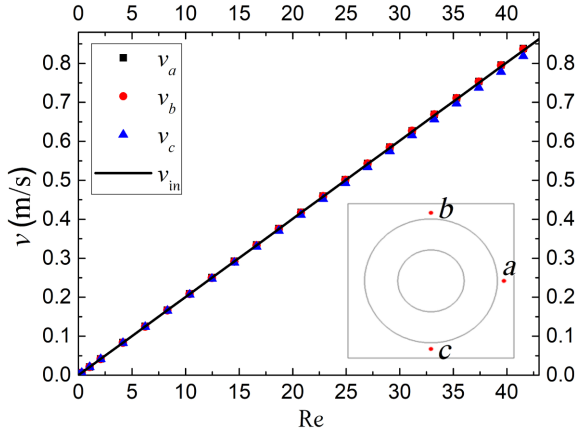

FIG. 4. Comparing y-component velocities near the outside cloak at $a(1.1R_2, 0)$, $b(0, 1.1R_2)$, and $c(0, -1.1R_2)$ with inlet velocity (v_{in}) on the $z = 0$ plane versus Re. Geometry with $H \times L \times D = 1$ cm $\times$ 1 cm $\times$ 50 μm, $R_1 = 2$ mm, and $R_2 = 4$ mm.

IV. EXPERIMENTAL SUGGESTIONS

To fabricate our cloak realistically in labs, researchers can thermally control the cloak, based on the fact that the dynamic viscosity depends on the temperature, to obtain the prescribed μ_{II} by using the formula of the water [38],

$$\mu = \mu_0 \exp\left[\frac{E}{R\,(T - T_0)}\right], \tag{7}$$

where $\mu_0 = 2.4055 \times 10^{-5}$ Pa s, $E = 4.753$ kJ/mol, $T_0 = 139.7$ K, and gas constant $R = 8.314$ J/(mol K). These viscosity values of the water calculated by Eq. (7) over a temperature interval of 273–463 K agree satisfactorily with experimental data [39–41]. Besides, we also consider the dependence of other fluid thermal properties, e.g., thermal conductivity, heat capacity, and density, on temperature. However, after laborious simulation exercises, we find that results in case A and those in case B appear almost identical, where case A denotes "only the viscosity depends on temperature, but the thermal conductivity, the heat capacity, and the density do not" and case B denotes "all thermal properties depend on temperature". This finding suggests that temperature effects on other thermal properties in our model can be neglected. Therefore, these characteristics allow users to readily manipulate flows simultaneously in experiments and computational simulations. According to Eq. (7), for water at room temperature $T_I = 293.15$ K, we can obtain $\mu_I = 1 \times 10^{-3}$ Pa s. According to Eq. (6), for $R_2 = 3.3$ mm and $R_1 = 2$ mm, we can obtain $\mu_{II} = 4.63 \times 10^{-4}$ Pa s. Finally, based on Eq. (7), we can obtain $T_{II} = 333.14$ K.Because of the shallowness of the flow field in z direction, the temperature distribution appears as a function of x and y only (nearly independent of z) if we prescribe the thermal boundary

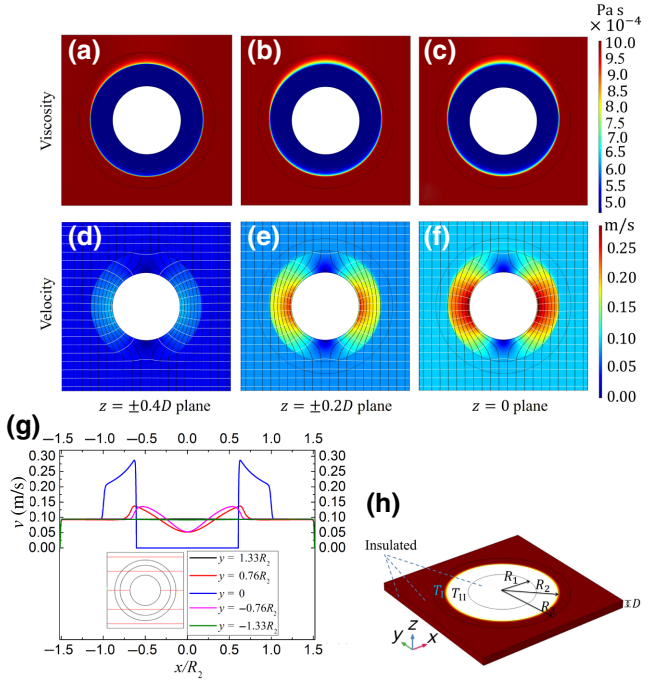

FIG. 5. Cloaking at Re = 4.51. Geometry with $H \times L \times D = 1$ cm $\times$ 1 cm $\times$ 50 μm, $R_1 = 2$ mm, $R_2 = 3.3$ mm, and $R_3 = 4$ mm. (a)–(c) Viscosity distributions of water on (a) $z = \pm 0.4D$ plane, (b) $z = \pm 0.2D$ plane, and (c) $z = 0$ plane. (d)–(f) Velocity distributions of water on (d) $z = \pm 0.4D$ plane, (e) $z = \pm 0.2D$ plane, and (f) $z = 0$ plane. (g) Velocity distributions at five different y positions on the $z = 0$ plane. Five red lines in the inset-figure model correspond to five legend-caption positions, respectively. (h) Thermally manipulating the viscosity of the cloak prescribed at $z = \pm 0.5D$.

condition merely on the $z = \pm 0.5D$ plane. For the prescription within $r \in [R_1, R_2]$, we set $T_{II} = 333.14$ K, and can rightfully obtain μ_{II} [Fig. 5(h)]. Because of the influence under the heat transfer, T_{II} will inevitably affect the viscosity of the freestream. For the purpose of eliminating this inevitable influence, we can manipulate $T_I = 293.15$ K within $r \in (R_2, R_3]$ on the $z = \pm 0.5D$ plane as the temperature of freestream does. Based on previously prescribed boundary conditions [Fig. 1(a) and 1(b)], the thermal boundary of the inlet is prescribed as $T = T_I$, and with the insulated condition elsewhere [Fig. 5(h)]. (Detailed boundary-condition settings are shown in Appendix A.) As a result, we are capable of constructing an intangible and nonintrusive cloak. Therefore, combining Eqs. (1) and (2) with the energy-transport equation,

$$\rho c_p \mathbf{u} \cdot \nabla T = \nabla \cdot (k \nabla T), \tag{8}$$

where c_p, k, and T denote heat capacity, thermal conductivity, and temperature, respectively. We can obtain viscosity and velocity distributions of water at Re = 4.51 on various planes [Figs. 5(a)–5(f)].

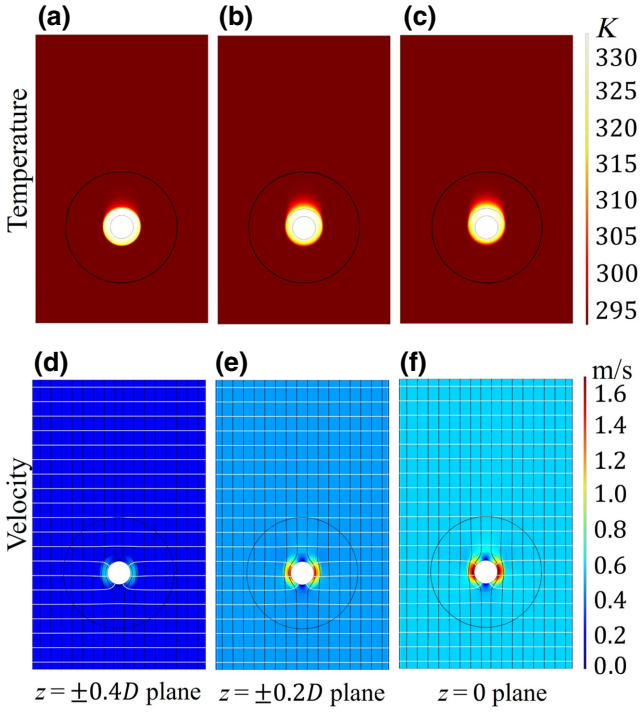

FIG. 6. Cloaking at Re = 27.97. Geometry with $H \times L \times D = 5$ cm $\times$ 3 cm $\times$ 50 μm, $R_1 = 2$ mm, $R_2 = 3.3$ mm, and $R_3 = 9.6$ mm. (a)–(c) Temperature distributions of water on (a) $z = \pm 0.4D$ plane, (b) $z = \pm 0.2D$ plane, and (c) $z = 0$ plane. (d)–(f) Velocity distributions of water on (d) $z = \pm 0.4D$ plane, (e) $z = \pm 0.2D$ plane, and (f) $z = 0$ plane.

In terms of viscosity or temperature values, which are one-to-one related, a gradual transition zone [Figs. 5(a)–5(c)], as opposed to an abrupt division between T_{I} and T_{II}, has been found to exist under the influence of the convection between the freestream and the cloak. In general, however, the viscosity computed by simulations agrees satisfactorily with that obtained by Eq. (6) from the analysis. In Figs. 5(d)–5(f), the orthogonality between isobars and streamlines is conspicuously observed, suggesting the physical realizability and validity of our analysis. Quantitatively, the velocity distribution outside the cloak appears uniform, confirming that it is unaffected by the presence of the obstacle [Fig. 5(g)].

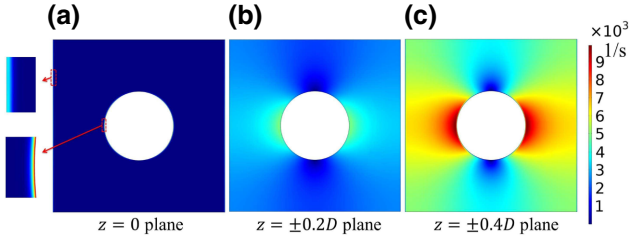

FIG. 7. Vorticity distributions ($\Omega = |\nabla \times \mathbf{u}|$) at Re = 4.51 on various planes for the obstacle-existent case.

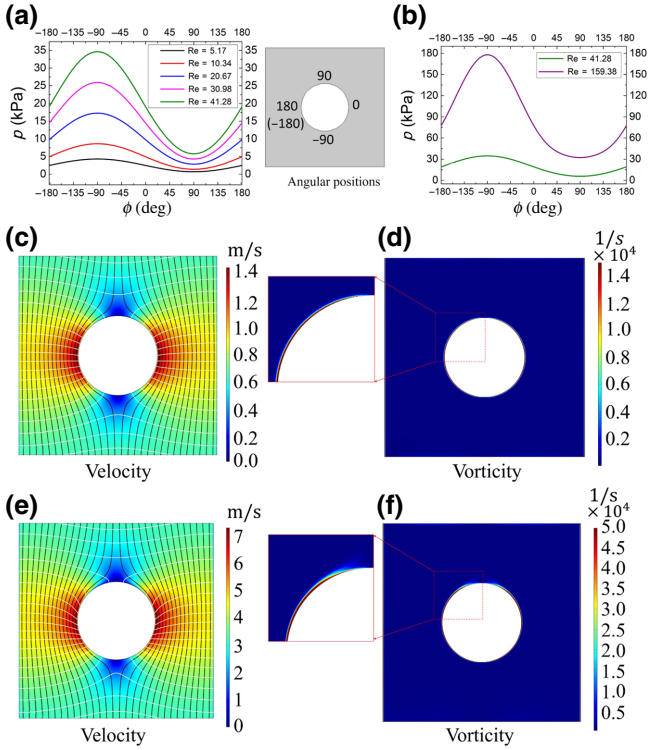

FIG. 8. (a),(b) Pressure distributions on the cylinder surface parameterized in several Reynolds numbers on the $z = 0$ plane for the obstacle-existent case. (c),(d) Velocity and vorticity distributions on the $z = 0$ plane at Re = 41.28. (e),(f) Velocity and vorticity distributions on the $z = 0$ plane at Re = 159.38. Geometry with $H \times L \times D = 1$ cm $\times$ 1 cm $\times$ 50 μm, $R_1 = 2$ mm.

To check the validity of our thermally controlled cloak at higher Re's, we choose the case Re = 27.97 as an example. Due to the existence of the convective heat transfer, the transition of the heat transfer between zone $(R_1, R_2]$ and zone $(R_2, R_3]$ strengthens as Re increases. To eliminate the influence of temperature T_{II}, we should increase the width of zone $(R_2, R_3]$ as Re increases. In Figs. 6(a)–6(c), even though a diffusive layer will be generated between two constant temperature regions in the fluid, the adverse low-temperature effect of the intrusively diffusive layer near the leading edge at $r = R_2$ is cancelled by the constructive high-temperature effect of the extrinsically diffusive layer near the trailing edge at $r = R_2$. After the obstacle-detoured effect of flows is cancelled, the high-temperature thermal energy of the extensionally diffusive layer near the trailing edge continues to be transported, but it merely strengthens the velocity of the flow by decreasing the viscosity. Therefore, if this zone is sufficiently widened to cool down the flow as the freestream of the obstacle-absent case is, the velocity outside this zone ($r > R_3$) will equal the freestream velocity of the obstacle-absent case, namely the orthogonality between isobars and streamlines is conspicuously observed [Figs. 6(d)–6(f)]. This trend implies

that, even if thermal diffusive layers proceed to exist in zone $(R_1, R_2]$ and zone $(R_2, R_3]$, our cloak remains valid.

Although we design the intangible hydrodynamic cloak for convective flows, the validity of our cloaks continues to be limited in the moderate range of Re's due to the rotational effect outside the boundary layer. To tackle much higher Reynolds-number problems in future studies, we are required to provide an external manipulating force, an external manipulating field, or other manipulating methods to exert on flows such that the rotational effect outside the boundary layer is cancelled.

V. CONCLUSIONS

Utilizing the convection-diffusion-balance method, we obtain uniform viscosities within the intangible hydrodynamic cloak. Our strategy, derived directly from Navier-Stokes equations, does not rely on the transformation theory, and thus evades troubles encountered in the past [30], exemplified by strict parameters (inhomogeneous and anisotropic) and intricate fabrication. Using these viscosities, we numerically demonstrate that Navier-Stokes flows can be manipulated by using the proposed cloak. Finally, our approach provides a guide for experiments, in which hydrodynamic cloaks are designed and fabricated.

ACKNOWLEDGMENTS

This work is funded by the China Postdoctoral Science Foundation under Grant No. 2019M661354, by the National Natural Science Foundation of China under Grants No. 11725521 and No. 12035004, as well as by the Science and Technology Commission of Shanghai Municipality under Grant No. 20JC1414700.

APPENDIX

1. Transforming Navier-Stokes equations into Laplace-equation form

Treating the viscosity as a constant value, Eqs. (1) and (2) can be written as

$$\nabla \cdot \mathbf{u} = 0, \tag{A1}$$

$$\rho \mathbf{u} \cdot \nabla \mathbf{u} + \nabla p = \mu \nabla^2 \mathbf{u}. \tag{A2}$$

For potential flows, we can introduce a velocity potential φ, such that $\nabla \varphi = \mathbf{u}$. According to Eq. (A1), we obtain

$$\nabla \cdot \nabla \varphi = 0, \tag{A3}$$

which is recognized as the Laplace equation.

According to the vector identity

$$\nabla \times (\nabla \times \mathbf{u}) = \nabla(\nabla \cdot \mathbf{u}) - \nabla^2 \mathbf{u}$$

and Eq. (A1), we can obtain

$$\nabla^2 \mathbf{u} = -\nabla \times (\nabla \times \mathbf{u}).$$

We take divergence $(\nabla \cdot)$ on both sides of the equation above and obtain

$$\nabla \cdot \nabla^2 \mathbf{u} = -\nabla \cdot [\nabla \times (\nabla \times \mathbf{u})] = 0.$$

According to Eq. (A2), we obtain

$$\nabla \cdot \mu^{-1}(\rho \mathbf{u} \cdot \nabla \mathbf{u} + \nabla p) = 0.$$

Utilizing another vector identity,

$$\mathbf{u} \cdot \nabla \mathbf{u} = \frac{1}{2} \nabla |\mathbf{u}|^2 - \mathbf{u} \times \nabla \times \mathbf{u},$$

we can obtain

$$\nabla \cdot \mu^{-1} \nabla \left(\frac{1}{2} \rho |\mathbf{u}|^2 + p \right) = 0,$$

$$\nabla \cdot \left(\mu^{-1} \nabla Q \right) = 0 \tag{A4}$$

for irrotational flows, where $Q = \frac{1}{2}\rho |\mathbf{u}|^2 + p$ is known as the mechanical-energy density with unit $\mathrm{J/m^3}$.

Therefore, Eqs. (A3) and (A4) can be written into

$$\nabla \cdot (\xi \nabla \Theta) = 0, \tag{A5}$$

which serves as a Laplace equation, where $\xi = (1, \mu^{-1})$ and $\Theta = (\varphi, Q)$.

2. The uniform viscosity of hydrodynamic cloaks deduced by convection-diffusion-balance method

The analytic solution of the Laplace equation $\nabla \cdot (\xi \nabla \Theta) = 0$ can be generally expressed as

$$\Theta_i = A_0^i + B_0^i \ln r + \sum_{m=0}^{\infty} \left[A_m^i \sin(m\theta) + B_m^i \cos(m\theta) \right] r^m + \sum_{m=0}^{\infty} \left[C_m^i \sin(m\theta) + D_m^i \cos(m\theta) \right] r^{-m}, \tag{A6}$$

where $A_0^i, B_0^i, A_m^i, B_m^i, C_m^i$, and D_m^i $(i = \mathrm{I}, \mathrm{II}, \mathrm{III})$ denote coefficients that will be determined by given boundary conditions.

Under physical boundary-condition constraints and finiteness of the computational domain, $m = 1$ and $A_1^i = C_1^i = B_0^i = 0$ should hold. As a result, Θ_i can be simplified as

$$\Theta_i = A_0^i + B_1^i r\cos\theta + D_1^i r^{-1}\cos\theta. \tag{A7}$$

Here Θ_i denotes solutions in different regions: $i = \mathrm{I}$ denotes the freestream regime ($r > R_2$); $i = \mathrm{II}$ the cloak layer ($R_1 < r \le R_2$); and finally $i = \mathrm{III}$ the cloaked regime ($r \le R_1$). Mathematically, at an interface, continuity conditions of

$$\begin{cases} \Theta_{\mathrm{III}}|_{r=R_1} = \Theta_{\mathrm{II}}|_{r=R_1} \\ \Theta_{\mathrm{II}}|_{r=R_2} = \Theta_{\mathrm{I}}|_{r=R_2} \\ \xi_{\mathrm{III}}\frac{\partial\Theta_{\mathrm{III}}}{\partial r}\Big|_{r=R_1} = \xi_{\mathrm{II}}\frac{\partial\Theta_{\mathrm{II}}}{\partial r}\Big|_{r=R_1} \\ \xi_{\mathrm{II}}\frac{\partial\Theta_{\mathrm{II}}}{\partial r}\Big|_{r=R_2} = \xi_{\mathrm{I}}\frac{\partial\Theta_{\mathrm{I}}}{\partial r}\Big|_{r=R_2} \end{cases} \tag{A8}$$

should prevail.

Because the solid obstacle can be equivalently treated as an effectively infinitely viscous fluid that stops flows, we deduce $\xi_{\mathrm{III}} = 0$, i.e., $\mu_{\mathrm{III}} = \infty$.

By substituting Eq. (A7) into Eq. (A8) and setting $D_1^{\mathrm{I}} = 0$, we can obtain the analytic expressions for ξ in regime II as

$$\xi_{\mathrm{II}} = \frac{R_2^2 + R_1^2}{R_2^2 - R_1^2}\xi_{\mathrm{I}}. \tag{A9}$$

According to Eq. (A4), we can obtain

$$\mu_{\mathrm{II}} = \frac{R_2^2 - R_1^2}{R_2^2 + R_1^2}\mu_{\mathrm{I}}. \tag{A10}$$

Boundary-condition setting:

At $x = \pm W/2$ wall, $u = v = 0$, nonslip wall.
At $z = \pm D/2$ wall, $u = v = 0$, nonslip wall.
At $r = R_1$ wall, $u = v = 0$, nonslip wall.
At $y = -H/2$, $p = p_2$, inlet.
At $y = H/2$, $p = p_1$, outlet.
At $z = \pm D/2$ and $r \le R_1$ wall, $\partial T/\partial z = 0$.
At $z = \pm D/2$ and $R_1 < r \le R_2$ wall, $T = T_{\mathrm{II}}$.
At $z = \pm D/2$ and $R_2 < r \le R_3$ wall, $T = T_{\mathrm{I}}$.
At $z = \pm D/2$ and $r > R_3$ wall, $\partial T/\partial z = 0$.
At $x = \pm W/2$ wall, $\partial T/\partial x = 0$.
At $y = -H/2$, $T = T_{\mathrm{I}}$, inlet (temperature boundary).
At $y = H/2$, $\partial T/\partial y = 0$, outlet (open boundary).

In Fig. 6, because the system is enlarged, coordinates of the inlet and the outlet $y = \pm H/2$ are replaced by $y = -H/6$ and $5H/6$, respectively.

[1] Ulf Leonhardt, Optical conformal mapping, Science **312**, 1777 (2006).
[2] Vladimir M. Shalaev, Transforming light, Science **322**, 384 (2008).
[3] Andrea Alu and Nader Engheta, Multifrequency Optical Invisibility Cloak with Layered Plasmonic Shells, Phys. Rev. Lett. **100**, 113901 (2008).
[4] Huanyang Chen, Che Ting Chan, and Ping Sheng, Transformation optics and metamaterials, Nat. Mater. **9**, 387 (2010).
[5] John B. Pendry, David Schurig, and David R. Smith, Controlling electromagnetic fields, Science **312**, 5781 (2006).
[6] David Schurig, J. J. Mock, B. J. Justice, Steven A. Cummer, John B. Pendry, A. F. Starr, and David R. Smith, Metamaterial electromagnetic cloak at microwave frequencies, Science **314**, 977 (2006).
[7] Allan Greenleaf, Yaroslav Kurylev, Matti Lassas, Ulf Leonhardt, and Gunther Uhlmann, Cloaked electromagnetic, acoustic, and quantum amplifiers via transformation optics, Proc. Natl. Acad. Sci. **109**, 10169 (2012).
[8] Fedor Gömöry, Mykola Solovyov, Ján Šouc, Carles Navau, Jordi Prat-Camps, and Alvaro Sanchez, Experimental realization of a magnetic cloak, Science **335**, 1466 (2012).
[9] Jianfei Zhu, Wei Jiang, Yichao Liu, Ge Yin, Jun Yuan, Sailing He, and Yungui Ma, Three-dimensional magnetic cloak working from DC to 250 khz, Nat. Commun. **6**, 8931 (2015).
[10] Huanyang Chen and C. T. Chan, Acoustic cloaking in three dimensions using acoustic metamaterials, Appl. Phys. Lett. **91**, 183518 (2007).
[11] Lucian Zigoneanu, Bogdan-Ioan Popa, and Steven A. Cummer, Three-dimensional broadband omnidirectional acoustic ground cloak, Nat. Mater. **13**, 352 (2014).
[12] Fan Yang, Zhong Lei Mei, Tian Yu Jin, and Tie Jun Cui, DC Electric Invisibility Cloak, Phys. Rev. Lett. **109**, 053902 (2012).
[13] T Bückmann, M Thiel, M Kadic, R Schittny, and M Wegener, An elasto-mechanical unfeelability cloak made of pentamode metamaterials, Nat. Commun. **5**, 4130 (2014).
[14] Tiemo Bückmann, Muamer Kadic, Robert Schittny, and Martin Wegener, Mechanical cloak design by direct lattice transformation, Proc. Natl. Acad. Sci. **112**, 4930 (2015).
[15] C. Z. Fan, Y. Gao, and J. P. Huang, Shaped graded materials with an apparent negative thermal conductivity, Appl. Phys. Lett. **92**, 251907 (2008).
[16] Sebastien Guenneau, Claude Amra, and Denis Veynante, Transformation thermodynamics: Cloaking and concentrating heat flux, Opt. Express **20**, 8207 (2012).
[17] Supradeep Narayana and Yuki Sato, Heat Flux Manipulation with Engineered Thermal Materials, Phys. Rev. Lett. **108**, 214303 (2012).
[18] Ying Li, Ke-Jia Zhu, Yu-Gui Peng, Wei Li, Tianzhi Yang, He-Xiu Xu, Hong Chen, Xue-Feng Zhu, Shanhui Fan, and C.-W. Qiu, Thermal meta-device in analogue of zero-index photonics, Nat. Mater. **18**, 48 (2019).
[19] Mohamed Farhat, Stefan Enoch, Sébastien Guenneau, and A. B. Movchan, Broadband Cylindrical Acoustic Cloak for Linear Surface Waves in a Fluid, Phys. Rev. Lett. **101**, 134501 (2008).
[20] Shu Zhang, Chunguang Xia, and Nicholas Fang, Broadband Acoustic Cloak for Ultrasound Waves, Phys. Rev. Lett. **106**, 024301 (2011).

[21] Siyuan Zou, Yadong Xu, Razafizana Zatianina, Chunyang Li, Xu Liang, Lili Zhu, Yongqiang Zhang, Guohua Liu, Qing Huo Liu, Huanyang Chen, and Zhenyu Wang, Broadband Waveguide Cloak for Water Waves, Phys. Rev. Lett. **123**, 074501 (2019).

[22] Shuang Zhang, Dentcho A. Genov, Cheng Sun, and Xiang Zhang, Cloaking of Matter Waves, Phys. Rev. Lett. **100**, 123002 (2008).

[23] Allan Greenleaf, Yaroslav Kurylev, Matti Lassas, and Gunther Uhlmann, Approximate Quantum Cloaking and Almost-Trapped States, Phys. Rev. Lett. **101**, 220404 (2008).

[24] Yaroslav A. Urzhumov and David R. Smith, Fluid Flow Control with Transformation Media, Phys. Rev. Lett. **107**, 074501 (2011).

[25] Yaroslav A. Urzhumov and David R. Smith, Flow stabilization with active hydrodynamic cloaks, Phys. Rev. E **86**, 056313 (2012).

[26] Patrick T. Bowen, David R. Smith, and Yaroslav A. Urzhumov, Wake control with permeable multilayer structures: The spherical symmetry case, Phys. Rev. E **92**, 063030 (2015).

[27] Dean R. Culver, Earl Dowell, David Smith, Yaroslav Urzhumov, and Abraham Varghese, A volumetric approach to wake reduction: Design, optimization, and experimental verification, J. Fluids **2016**, 1 (2016).

[28] Gaole Dai, Jin Shang, and Jiping Huang, Theory of transformation thermal convection for creeping flow in porous media: Cloaking, concentrating, and camouflage, Phys. Rev. E **97**, 022129 (2018).

[29] Gaole Dai and Jiping Huang, A transient regime for transforming thermal convection: Cloaking, concentrating, and rotating creeping flow and heat flux, J. Appl. Phys. **124**, 235103 (2018).

[30] Juhyuk Park, Jae Ryoun Youn, and Young Seok Song, Hydrodynamic Metamaterial Cloak for Drag-Free Flow, Phys. Rev. Lett. **123**, 074502 (2019).

[31] Fuyang Tay, Youming Zhang, Hongyi Xu, Honghui Goh, Yu Luo, and Baile Zhang, A metamaterial-free fluid-flow cloak, arXiv:1908.07169 (2019).

[32] John Conrad Jaeger and Horatio Scott Carslaw, *Conduction of Heat in Solids* (Clarendon Press, Oxford, 1959).

[33] Yungui Ma, Yichao Liu, Muhammad Raza, Yudong Wang, and Sailing He, Experimental Demonstration of a Multiphysics Cloak: Manipulating Heat Flux and Electric Current Simultaneously, Phys. Rev. Lett. **113**, 205501 (2014).

[34] Tiancheng Han, Xue Bai, Dongliang Gao, John T. L. Thong, Baowen Li, and Cheng-Wei Qiu, Experimental Demonstration of a Bilayer Thermal Cloak, Phys. Rev. Lett. **112**, 054302 (2014).

[35] Hongyi Xu, Xihang Shi, Fei Gao, Handong Sun, and Baile Zhang, Ultrathin Three-Dimensional Thermal Cloak, Phys. Rev. Lett. **112**, 054301 (2014).

[36] Henry Selby Hele-Shaw, The flow of water, Nature **58**, 34 (1898).

[37] Pijush K. Kundu, David R. Dowling, Grétar Tryggvason, and Ira M. Cohen, *Fluid Mechanics* (Academic Press, Berlin, 2015).

[38] R. L. Fogel'son and E. R. Likhachev, Temperature dependence of viscosity, Tech. Phys. **46**, 1056 (2001).

[39] J. R. Coe Jr and T. B. Godfrey, Viscosity of water, J. Appl. Phys. **15**, 625 (1944).

[40] M. P.o Vukalovich, S. L. Rivkin, and A. A. Aleksandrov, Tables of thermophysical properties of water and steam, Standartov, Moscow **408**, 1 (1969).

[41] Lawrence Korson, Walter Drost-Hansen, and Frank J. Millero, Viscosity of water at various temperatures, J. Phys. Chem. **73**, 34 (1969).